EurJIC European Journal of Inorganic Chemistry

ChemPubSoc Europe

FULL PAPER

DOI:10.1002/ejic.201402160

Mono- and Dinuclear Complexes of Tricarbonylrhenium(I) with 4-Methyl-2,2′-bipyridine-4′-carbonitrile

Juan H. Mecchia Ortiz,[a] Faustino E. Morán Vieyra,[b] Claudio D. Borsarelli,[b] Isabel Romero,[c] Xavier Fontrodona,[c] Teodor Parella,[d] Noemí D. Lis de Katz,[a] Florencia Fagalde,[a] and Néstor E. Katz*[a]

Keywords: Rhenium / Ruthenium / Coordination chemistry / Electron transfer / Density functional calculations

Novel mono- and dinuclear tricarbonylrhenium(I) complexes of formula [Re(Mebpy-CN)$(CO)_3$Cl] (**1**), [Re(Mebpy-CN)-$(CO)_3(CH_3CN)$](PF_6) (**2**), and [$(CH_3CN)(CO)_3$Re(Mebpy-CN)$Ru(NH_3)_5$]$(PF_6)_3$ (**3**), in which Mebpy-CN = 4-methyl-2,2′-bipyridine-4′-carbonitrile, were prepared and characterized by spectroscopic, photophysical, and computational techniques. The complete structure of complex **2** was determined by X-ray diffraction. The increased conjugation in the bipyridyl ring owing to the nitrile substituent increases the emission quantum yields of the ^{3}MLCT (metal-to-ligand charge-transfer) lowest-lying excited states of **1** and **2** with respect to the corresponding bpy complexes (bpy = 2,2′-bipyridine). The mixed-valent species of formula [$(CH_3CN)(CO)_3$Re(Mebpy-CN)$Ru(NH_3)_5$]$^{4+}$ (**4**) was prepared in situ and as a mixed salt; the charge recombination from its metal-to-metal charge-transfer (MMCT) excited state is predicted to lie in the Marcus inverted region. The electronic structures and optical properties of all the reported complexes calculated by DFT and TD-DFT methods agree reasonably well with experimental results.

Introduction

Tricarbonylpolypyridylrhenium(I) complexes of the type [Re(diimine)$(CO)_3$(L)]$^{n+}$ have attracted great interest owing to their rich manifold of ground- and excited-state physicochemical properties. Structural variations of the diimine and/or the axial ligand L have led to applications of these complexes as sensors,[1] molecular switches,[2] probes for cell imaging,[3] in photochromism,[4] and for CO_2 reduction.[5] Dinuclear mixed-valent asymmetric complexes are relevant in the study of energy and electron-transfer processes.[6]

We have recently reported the syntheses and spectroscopic, electrochemical, spectroelectrochemical, and photophysical properties of a series of ruthenium polypyridyl complexes with 4-methyl-2,2′-bipyridine-4′-carbonitrile (Mebpy-CN) as an auxiliary ligand, the structure of which is shown in Scheme 1. An improvement in the photosensitizing properties with respect to [Ru(bpy)$_3$]$^{2+}$ (bpy = 2,2′-

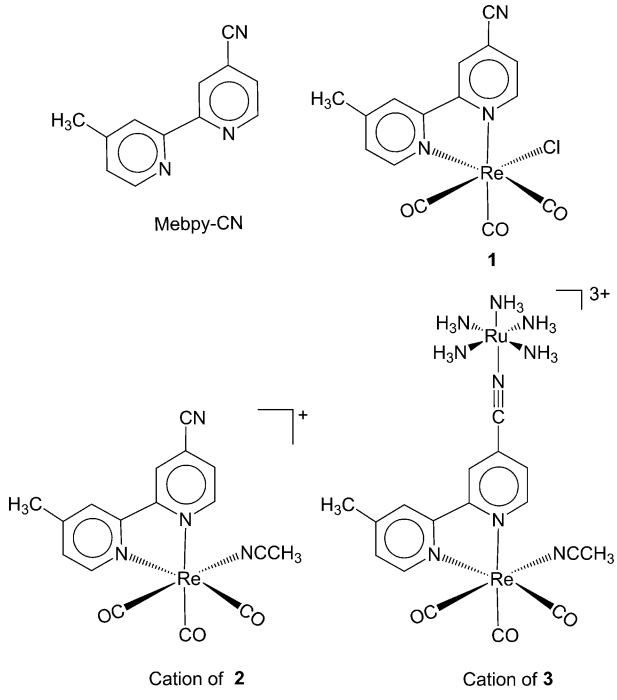

Scheme 1. Structures of Mebpy-CN; complex **1** and cations of **2** and **3**.

[a] INQUINOA-CONICET, Instituto de Química Física, Facultad de Bioquímica, Química y Farmacia, Universidad Nacional de Tucumán,
Ayacucho 471, T4000INI San Miguel de Tucumán, Argentina
E-mail: nkatz@fbqf.unt.edu.ar
www.inquinoa.org.ar
[b] Laboratorio de Cinética y Fotoquímica, Centro de Investigaciones y Transferencia de Santiago del Estero (CITSE-CONICET), Universidad Nacional de Santiago del Estero,
RN 9, Km 1125, 4206 Santiago del Estero, Argentina
[c] Departament de Química and Serveis Tècnics de Recerca, Universitat de Girona, Campus de Montilivi,
17071 Girona, Spain
[d] Servei de RMN, Universitat Autònoma de Barcelona, Bellaterra, 08193 Barcelona, Spain

Supporting information for this article is available on the WWW under http://dx.doi.org/10.1002/ejic.201402160.

bipyridine) was found when going from $x = 1$ to $x = 3$ in the series $[Ru(bpy)_{3-x}(Mebpy\text{-}CN)_x]^{2+}$ as a consequence of the increasing electronic delocalization imposed by the nitrile substituent on the bpy ring.[7]

To discover if this improvement can be reproduced in similar complexes with other transition metals, we report in this work the synthesis and spectroscopic, photophysical, and structural properties of new mono- and dinuclear tricarbonylrhenium(I) complexes of formula $[Re(Mebpy\text{-}CN)(CO)_3Cl]$ (**1**), $[Re(Mebpy\text{-}CN)(CO)_3(CH_3CN)]^+$, cation of **2**, $[(CH_3CN)(CO)_3Re(Mebpy\text{-}CN)Ru(NH_3)_5]^{3+}$, cation of **3**, and $[(CH_3CN)(CO)_3Re(Mebpy\text{-}CN)Ru(NH_3)_5]^{4+}$, cation of **4**. The experimental results will be compared with computational analysis using DFT and TD-DFT techniques. Chemical structures of **1** and the cations of **2** and **3** are also shown in Scheme 1.

Results and Discussion

Synthesis and Crystal Structure

The synthetic procedures used were similar to those previously described for related tricarbonylpolypyridylrhenium(I) complexes.[1,2,8] The new complexes were soluble in organic solvents, and their purity was confirmed by chemical analyses, IR, Raman, and NMR spectra.

The crystal structure of complex **2** was solved by X-ray diffraction analysis. The complex crystallizes with a molecule of toluene that interacts with Mebpy-CN through a π–π stacking interaction. This interaction is favored by the electron-withdrawing nature of the nitrile group in Mebpy-CN and the electron-donor nature of the methyl group of toluene. A face-centered stacking is the more favored orientation caused by this kind of interaction,[9] but the steric constraints imposed by the other molecules onto the crystal shift the position of the toluene ring.

Figure 1 displays the molecular structure of the cation of **2**, whereas the main crystallographic data and selected bond lengths and angles can be found in Tables S1 and S2 in the Supporting Information, respectively. The structure is that of a slightly distorted octahedron. All bond lengths and angles are within the expected values for tricarbonylpolypyridylrhenium(I) complexes; for example, the Re–N(py) mean distance in related complexes is 2.176 and 2.185 Å.[2] However, it is interesting to note that the Re1–N1 bond length, in which the pyridyl ring contains the nitrile group (2.162 Å), is slightly shorter than the distance found for Re–N2 (2.173 Å), in which the pyridyl ring contains the CH_3 group. This result is consistent with the optimized structure in the DFT calculations and is related to the electron-withdrawing effect of the CO groups that reinforces the Re–N bonding.

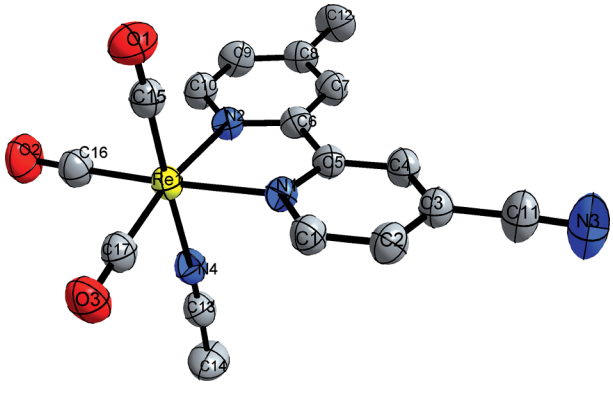

Figure 1. ORTEP diagram (ellipsoids at 70% probability) of the cation of **2** with C atoms in black, N atoms in blue, and Re atom in yellow. All hydrogen atoms have been omitted for clarity.

The N1–Re1–N2 angle of around 74° indicates the geometrical restrictions imposed by the bidentate pyridyl ligands; consequently, the rest of the equatorial angles for N–Re–CO are larger than 90°, which is expected for an ideal octahedral geometry. Finally, the distance C≡N (1.140 Å) is typical of nitrile bonded to an aromatic ring.[10]

IR, Raman, and NMR Spectra

IR spectra of complexes **1**–**4** exhibit the typical vibrational modes of bipyridine groups between 1650 and 1400 cm^{-1}, the characteristic band that corresponds to the υ(C≡N) stretching mode in Mebpy-CN, and the expected three bands of υ(C≡O), which correspond to the carbonyl stretching modes for Re complexes in the facial (*fac*) configuration.[11,12] A list of the wavenumbers is shown in the Exp. Section. The υ(C≡N) bands of **1** and **2**—more intense in the Raman than in the IR—are slightly displaced to higher wavenumbers with respect to that of the free ligand [υ(C≡N) = 2234 cm^{-1}], a shift that can be attributed to metal coordination to the pyridine nitrogen atoms of Mebpy-CN, as reported before for similar Ru complexes.[7,13] In these complexes, since no π backdonation from the metal center to the nitrile group is expected owing to their remote interaction, υ(C≡N) is shifted to a higher frequency as a result of the inductive effect of the metal.[11] The lower value of υ(C≡O) in **1** with respect to **2** is due to the fact that Cl^- is a weaker π acceptor than CH_3CN, and therefore the extent of π backbonding from Re^I to the carbonyls is higher in **1** than in **2**.

The coordination of the $[Ru(NH_3)_5]^{2+}$ group to the nitrile end of coordinated Mebpy-CN in complex **3** is confirmed by the considerable shift of υ(C≡N) to a lower value than that of the free ligand ($\Delta\upsilon$ = –55 cm^{-1}) as a consequence of the strong π-backbonding effect from d_π orbitals of ammine Ru to π* orbitals of Mebpy-CN.[7] This effect increases the π backbonding of Re^I to the π* orbitals of the carbonyl groups and the nitrile end of acetonitrile, which shifts the corresponding υ(C≡O) and υ(C≡N) bands to lower wavenumbers. The ammonia symmetric deformation mode of **3** appears at $\delta_{sym}(NH_3)$ = 1278 cm^{-1}, thus indicating the oxidation state(II) of the Ru center.[13]

Assignments of all NMR spectroscopic signals could be carried out by 2D techniques and are displayed in the Exp. Section.

UV/Vis Spectra

The UV/Vis spectra of complexes **1**–**3** in CH_3CN at room temperature are shown in Figure 2. Data of λ_{max} and ε_{max} are included in the Exp. Section. Intraligand transitions are observed between 200 and 300 nm. All the complexes exhibit $d_\pi(Re) \rightarrow \pi^*$ (Mebpy-CN) metal-to-ligand charge transfer (MLCT) bands at λ_{max} = 402, 360, and 358 nm for **1**, **2**, and **3**, respectively. By substituting Cl^- by the more π-accepting acetonitrile, the MLCT band is shifted to higher energies. The band centered at λ_{max} = 516 nm in **3** corresponds to a $d_\pi(Ru) \rightarrow \pi^*$ (Mebpy-CN) MLCT band, which disappears upon oxidizing Ru^{II} to Ru^{III} by adding bromine or by applying an adequate potential (1 V). Figure 3 shows a spectroelectrochemical experiment of **3**. A metal-to-metal charge transfer (MMCT) band is detected at λ_{max} = 577 nm in complex **4**.

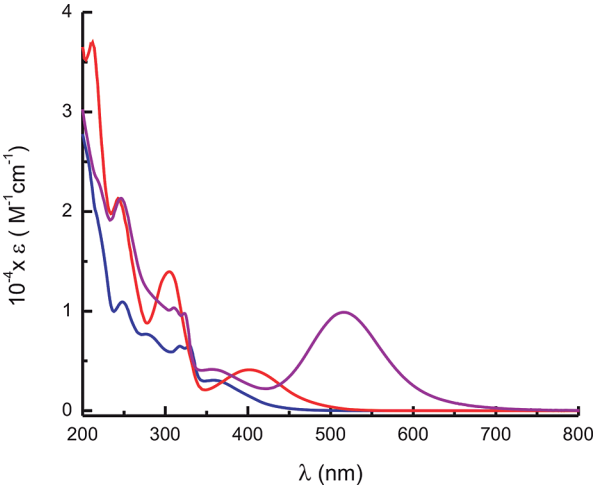

Figure 2. UV/Vis spectra of **1** (red line), **2** (blue line), and **3** (purple line) in CH_3CN at room temperature.

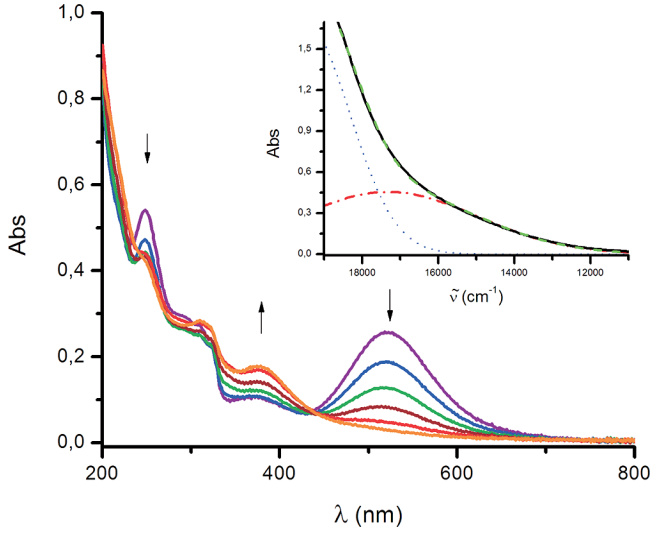

Figure 3. UV/Vis spectra obtained by controlled potential electrolysis of **3** at 1 V versus Ag/AgCl in CH_3CN, the final species being **4**. Inset: 3.45×10^{-3} M solution of **3** in CH_3CN (black line) after addition of an excess amount of Br_2(g). Red dash-dot line: MMCT band obtained by deconvolution; green dashed line: fitted spectra.

Electrochemistry and Spectroelectrochemistry

Values of the redox potentials of the cations of complexes **1**–**3** in CH_3CN [0.1 M tetrakis(*n*-butyl)ammonium hexafluorophosphate (TBAH)] versus Ag/AgCl (3 M KCl) obtained by cyclic voltammetry are shown in Table 1. The oxidations of the rhenium centers in all complexes are quasi-reversible. For complex **1**, a fast substitution of Cl^- by CH_3CN occurs upon oxidation by means of a disproportionation mechanism.[14a] The first reduction wave of **1** is reversible and is followed by two consecutive reduction processes, one reversible and the other irreversible,[14b] as shown in Figure 4. The spectroelectrochemical behavior of **1** at an applied potential V = –1 V reveals that after reduction of the ligand and reoxidation, Cl^- is labilized and substituted by CH_3CN and the nitrile group of Mebpy-CN is hydrolyzed to amide. Evidence of this transformation has been obtained by spectroscopic measurements. As shown in Figure S1 of the Supporting Information, the UV/Vis spectrum of the electrolyzed solution is the same as that obtained from a hydrolyzed sample obtained by column purification and identified by its IR spectrum shown in Figure S2 of the Supporting Information: the ν(C≡N) band of **1** disappears completely and a new and intense band appears at 1686 cm^{-1}, which is typical of a carbonyl stretching vibration of a carboxamide group.[11] Nitrile hydrolysis is also observed in the dinuclear complex **4**, as discussed below.

Table 1. Electrochemical data, in CH_3CN, at 22 °C.[a]

	$E^{ox}_{1/2}$ [V]	$E^{red}_{1/2}$ [V]	$\Delta E_{1/2}$ [V][b]	10^{-4} ν_{MLCT} [cm^{-1}]
1	1.43	–0.97, –1.22, –1.30	2.40	2.49
2	1.87	–0.85, –1.18, –1.28	2.72	2.78
3	1.91, 0.75	–0.90, –1.34, –1.47	2.81, 2.11	2.79, 1.94

[a] $E_{1/2}$ versus Ag/AgCl. [b] $\Delta E_{1/2} = E^{ox}_{1/2} - E^{red1}_{1/2}$.

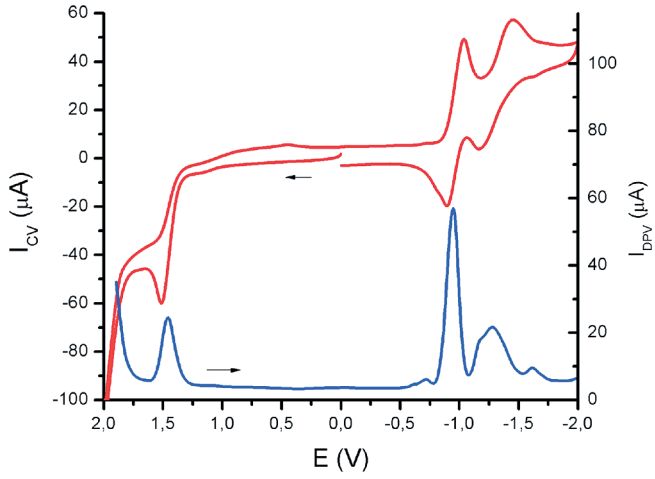

Figure 4. Cyclic voltammogram (in red) and differential pulse voltammogram (in blue) for complex **1** in CH_3CN, 0.1 M TBAH.

For the cation of complex **2**, in which Cl^- is replaced by CH_3CN, the redox potential of the metallic couple Re^{2+}/Re^+ is higher than that in **1** owing to the lower electron-donor character and higher π-acceptor capability of CH_3CN. Its first reduction wave ($E_{1/2}$ = –0.85 V) is reversible and followed by two reduction process (one reversible and the other irreversible). The UV/Vis spectroelectrochemistry of the cation of complex **2** at an applied potential of V = –0.9 V is displayed in Figure 5: a bleaching of the MLCT band at 350 nm and appearance of new bands at 370 and 450 nm are observed, consistent with the formation of the radical anion Mebpy-$CN^{\bullet-}$. Reoxidation at V = –0.7 V produces almost a total recovery of the original complex.

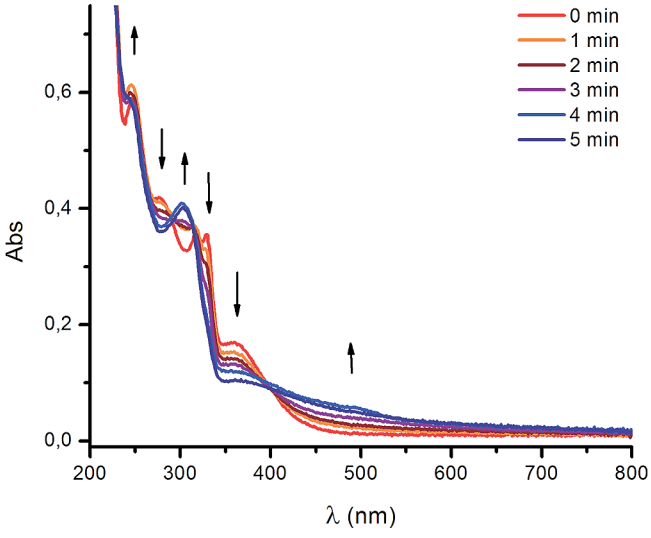

Figure 5. UV/Vis spectroelectrochemistry of **2** in CH_3CN, 0.1 M TBAH at V = –0.9 V.

The dimetallic cation of complex **3** has a higher redox potential for the rhenium couple than that of **2**, as expected when considering its higher charge. The redox potential of the ruthenium couple Ru^{3+}/Ru^{2+} ($E_{1/2}$ = 0.75 V) is characteristic of nitrile species coordinated to pentaammineruthenium groups.[7]

There is a correspondence between the electrochemical data and the positions of the MLCT bands, as expected.[15] In effect, a linear relationship is disclosed (see Table 1) between $\Delta E_{1/2} = E^{ox}_{1/2} - E^{red1}_{1/2}$ and the maximum frequency of the MLCT bands, ν_{MLCT}.

Kinetics of Nitrile Hydrolysis

In aqueous solutions, complex **4** undergoes nitrile hydrolysis, as evidenced by the consecutive UV/Vis spectra shown in Figure S3 of the Supporting Information. When oxidizing complex **3** to complex **4** by adding $K_2S_2O_8$ in an excess amount at pH = 3.0 (CF_3COOH) and I = 0.1 M (KCl), the MLCT band is displaced to higher energies, as expected when the nitrile group is hydrolyzed to a carboxamide group.[16] The rate constant obtained under pseudo-first-order conditions after triplicate measurements, k_h = $(2.5 \pm 0.5) \times 10^{-2}$ s^{-1}, is of the expected order for mixed-metal complexes in which a nitrile group of a bridging ligand is coordinated to Ru^{III}.[16]

Intramolecular Electron Transfer

Coordination of a pentaammineruthenium(II) moiety to the free N of the nitrile group of Mebpy-CN bonded to the $[Re(CO)_3(CH_3CN)]^+$ core is clearly evidenced in the cation of complex **3** by IR, cyclic voltammetry (CV), and UV/Vis data. As shown in Figure 3, selective oxidation of the ruthenium center in **3** either by an electrochemical or a chemical method produces the mixed-valent complex **4**. The band at λ_{max} = 516 nm that corresponds to the MLCT transition $d_\pi(Ru) \rightarrow \pi^*$(Mebpy-CN) disappears and a weak band appears at λ_{max} = 577 nm (ε = 132 $M^{-1}cm^{-1}$) that corresponds to an MMCT transition $d_\pi(Re^I) \rightarrow d_{\pi^*}(Ru^{III})$. The experimental values of $\tilde{\nu}_{max}$, ε_{max}, and E_{op} obtained by deconvolution of the Gaussian-shaped MMCT band (inset of Figure 3) can be used to calculate the values of H_{AB}, α^2, and λ (electronic coupling, electron delocalization parameter, and reorganization energy for the intramolecular metal-to-metal electron transfer, respectively) through Equations (1), (2), and (3)[17]

$$H_{AB}\,(cm^{-1}) = 2.06 \times 10^{-2}\,[(\varepsilon_{max})(\tilde{\nu}_{max})(\Delta\tilde{\nu}_{1/2})]^{1/2}\,(1/r) \quad (1)$$

$$\alpha^2 = (H_{AB}/\tilde{\nu}_{max})^2 \quad (2)$$

$$\lambda = E_{op} - \Delta G^{o} - \Delta E_{exc} \quad (3)$$

in which ε_{max} is the molar absorptivity at the absorption maximum, $\tilde{\nu}_{max}$ is the energy of the intervalence absorption maximum, $\Delta\tilde{\nu}_{1/2}$ is the bandwidth at half-height of the intervalence transition, r is the metal–metal distance, E_{op} is the energy of the intervalence absorption maximum in eV, $\Delta G°$ is the free energy between both redox centers [assumed as approximately $\Delta E_{1/2} = E_{1/2}(Re^{II}/Re^I) - E_{1/2}(Ru^{III}/Ru^{II})$], and ΔE_{ex} is the energy difference between the excited and ground states, estimated as 0.25 eV for several ruthenium complexes in the event that the MMCT transition results in the population of an excited state.[18] The distance r (9.425 Å) was estimated on the basis of the crystal structure of **2** and the typical Ar–CN–$Ru(NH_3)_5$ distance.[13] The value of the estimated electronic coupling element between both metallic centers calculated with Equation (1), H_{AB} = 484 cm^{-1}, is similar to that found for a mixed-valent complex with a comparable metal–metal distance, of formula $[(bpy)_2Ru(Mebpy\text{-}CN)Ru(NH_3)_5]^{5+}$.[7] The value of α^2 (7.8×10^{-4}) indicates a similar delocalization. The value of the reorganization energy λ (=0.74 eV) is less than that of $-\Delta G°$ (= 1.16 eV) so that the rate constant for the charge-recombination step following light excitation ($Ru^{II} \rightarrow Re^{II}$)

(k_b in Scheme 2) is predicted to fall in the Marcus inverted region.[19] This fact opens up the possibility of having long-lived charge-separated states in mixed-valence chemistry.

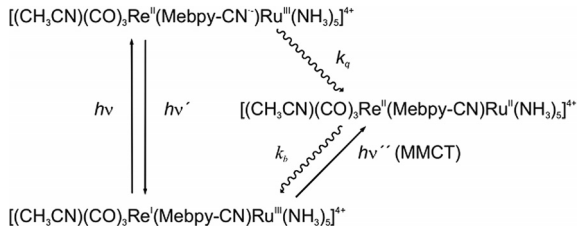

Scheme 2. Formation of the mixed-valent isomer of **4** by light excitation. Straight arrows indicate radiative processes; curved arrows indicate nonradiative processes.

Photophysical Properties

Relative radiative quantum yields were calculated by using Equation (4)

$$\varphi_x = \varphi_r \frac{(I_x/A_x)}{(I_r/A_r)}\left(\frac{\eta_x}{\eta_r}\right)^2 \quad (4)$$

in which Φ_r is the quantum yield of a reference ([Ru(bpy)$_3$](PF$_6$)$_2$ in acetonitrile, $\Phi_r = 0.095$),[20] I_r and I_x are the integrated sums of the emission intensities of the reference and the sample, respectively, A_x and A_r are the absorbances of the sample and the reference at their excitation wavelengths, and η_x and η_r are the refraction indexes of the respective solvents (taken to be equal to the neat solvents).

Estimates of the zero-point energy gap (E_0), the Huang–Rhys factor (S_M), the energy of the average vibrational mode coupling of the ground and excited states ($\hbar\omega_M$), and the spectral bandwidth ($\Delta\nu_{0,1/2}$) were determined by a single-mode fit of the steady-state emission spectra according to Equation (5) as described by Meyer et al.[21]

$$I(\tilde{\nu}) = \sum_{\nu=0}^{10}\left\{\left(\frac{E_0 - \nu_M\hbar\omega_M}{E_0}\right)^4 \frac{S_M{}^{\nu_M}}{\nu_M!}\exp\left(-4\ln(2)\left(\frac{\tilde{\nu} - E_0 + \nu_M\hbar\omega_M}{(\Delta\nu_{0,1/2}}\right)^2\right\}\right. \quad (5)$$

Figure 6 shows the normalized spectral traces for emission of complexes **1**–**4** at room temperature using this equation. Their emission manifold even at 77 K is broad and unstructured, as is typical for decays from ^{3}MLCT excited states of tricarbonypolypyridylrhenium(I) complexes.[12] The values of $\hbar\omega_M$ obtained from fitting at 77 K were used in the fitting at room temperature. The spectral fitting results for all the complexes are shown on Table S3 of the Supporting Information.

The electron-vibrational coupling constants (Huang–Rhys factors) are dimensionless quantities related to the difference in equilibrium displacement for the normal modes (ΔQ_e) between the ground state and excited state as stated in Equation (6)

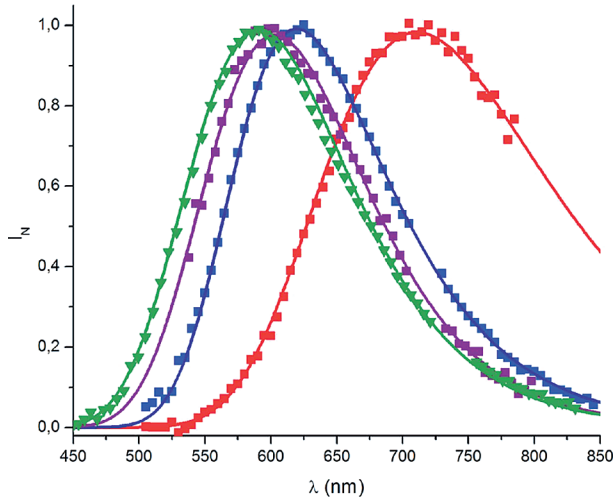

Figure 6. Spectral fitting of normalized emission spectra of complexes **1** (red), **2** (blue), **3** (purple), and **4** (green) using Equation (5) (λ_{exc} = 350 nm).

$$S_M = 1/2(M\omega/\hbar)(\Delta Q_e)^2 \quad (6)$$

in which M is the reduced mass and ω the angular frequency ($2\pi\nu$) for the normal mode. The values of S_M decreases when going from **1** to **4**, thus indicating that the rigidity of Mebpy-CN increases along the series. The S_M factor is smaller for Mebpy-CN complexes than for bpy complexes, a fact that can be explained by the increased electronic delocalization induced by the nitrile group.[22]

The photophysical properties of complexes **1**–**4** in CH$_3$CN at room temperature are summarized in Table 2. The quantum yield of complex **3** is less than that of complex **2** because the absorption maximum of the Ru chromophore (λ_{abs} = 516 nm) is close to the emission maximum of the excited Re chromophore (λ_{em} = 588 nm), thus leading to an "autoquenching" process. However, the luminescence lifetime of **3** is longer than that of **2** because of the increased delocalization caused by the coordination of the N end of the nitrile group of the bridging ligand to the Ru center in **3**. The increase in the excited-state lifetime when going from **1** to **4** parallels the decrease in S_M. The shift to lower energies of the excited states in Mebpy-CN complexes relative to the bpy complexes can explain the increase in k_{nr} values and the subsequent decrease in the corresponding lifetimes

Table 2. Photophysical properties of the excited states of complexes **1**–**4**, in CH$_3$CN, at room temp (* indicates an excited state).

	τ [ns][a]	τ [ns][b]	Φ	10^{-5} k_r [s^{-1}][a]	10^{-7} k_{nr} [s^{-1}][c]
1*	12	–	0.0020	1.6	8.1
2*	286	293	0.085	3.0	3.2
3*	439	431	0.0046	0.10	0.23
4*	31 (12%), 482 (88%)	91 (47%), 480 (53%)	0.046	0.95	0.20

[a] Time-correlated single-photon counting (TCSPC). [b] Laser flash photolysis (LFP). [c] $k_{nr} = k_{obs} - k_r$.

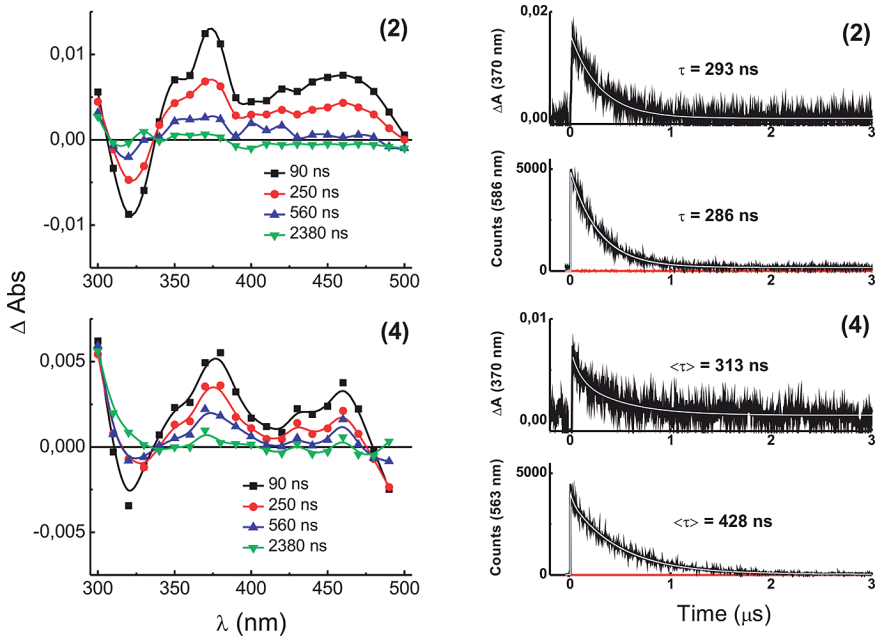

Figure 7. Transient spectra for complexes **2** and **4** in CH_3CN at room temp. together with the transient absorption decays monitored at 370 nm (top), and the emission decays obtained by TCSPC and monitored at the emission maximum (bottom) of each complex. Solid gray lines represent mono- (complex **2**) and double- (complex **4**) exponential fitting.

according to the energy-gap law.[12] However, the quantum yields of luminescence for Mebpy-CN complexes are higher than those of the corresponding bpy complexes (e.g., for $[Re(bpy)(CO)_3(CH_3CN)]^{+*}$, $\phi = 0.0225$),[23] a fact that has been previously detected for ruthenium complexes with Mebpy-CN[7] and can be attributed to the increased electron delocalization in the bpy ring that occurs upon adding a nitrile group.

The transient spectra and absorbance decay at 370 nm for complexes **2** and **4** are shown in Figure 7. For complex **4**, no evidence of the formation of a transient Ru^{II} species was obtained in the LFP experiments, since the emission of the excited state at 579 nm interferes with the possible transient absorption near 520 nm; therefore, the spectra were cut off at 500 nm. The observed maxima at 370 and 450 nm can be assigned to IL transitions of the Mebpy-$CN^{\cdot-}$ radical, in agreement with the spectroelectrochemical results obtained upon reduction of Mebpy-CN (Figure 5) and with previous studies on Ru complexes.[7] The transient decays are compared with the emission decays of both complexes obtained by TCSPC and monitored at the emission maximum of each complex. For complex **2**, and also for complex **3** (not shown), the observed decays were perfectly monoexponential, and both transient techniques yielded the same lifetime for each complex (see Table 2). In contrast, the absorption and emission decays for complex **4** showed double-exponential decay behavior. The data were fitted with the general function $Y(t) = a_1\exp(-t/\tau_1) + a_2\exp(-t/\tau_2)$ with $a_1 + a_2 = 1$, and to compare both techniques, the average lifetime was calculated as $<\tau> = a_1\tau_1 + a_2\tau_2$. The longer lifetime obtained by both methods was the same and closer to that observed for complex **3** (owing to the decay from the ^{3}MLCT excited state [Re^{II}Mebpy-$CN^{\cdot-}$]), but a little difference was obtained for the shorter decay component between both techniques. This result can be attributed to the noisier LFP than TCSPC signal and also to different monitoring wavelengths. Despite this, a decay that is one order of magnitude faster is present for complex **4** that can be attributed to an extra nonradiative pathway as shown in Scheme 2. Now, since it is well known that the lifetimes of non-emissive charge-transfer excited states of tricarbonylpolypyridylrhenium(I) complexes usually fall in the nanosecond regime,[24] we propose that the shorter lifetime could be due to the decay from an excited MMCT state: the charge recombination process, k_b, shown in Scheme 2, which has been predicted to lie in the Marcus inverted region.

Calculations

Table 3 shows the compositions of some frontier MOs for complexes **1**–**4**. There is a remarkable mixing between the d_π(Re) and the d_π(Cl) orbitals in the HOMO of **1**. Therefore, the lowest-lying energy absorption band in **1** can be assigned to a metal–ligand-to-ligand charge transfer (MLLCT) transition. The electron-density difference map (EDDM) for this band can be envisaged as a transfer of electronic density from the $Re(CO)_3Cl$ fragment to Mebpy-CN, as described for $[Re(bpy)(CO)_3Cl]$ by Vlček and Záliš.[25a] In the whole series, the LUMO is centered at the Mebpy-CN ligand. In the mixed-valent complex **4**, the α- and β-MO compositions are displayed. It is well known that in molecules with unpaired electrons, the spin orbitals are spin-unrestricted and therefore the spatial parts of the α orbitals will differ from the spatial parts of the β orbit-

als.[25b] In this case, the β-spin LUMO orbital is centered on the Ru atom, which is consistent with the experimental description of the mixed-valent species as $[(CH_3CN)(CO)_3Re^{I}(Mebpy\text{-}CN)Ru^{III}(NH_3)_5]^{4+}$. Diagrams of LUMOs and HOMOs for all complexes are displayed in Figure 8.

Table 3. Energies and percent contributions of the three highest HOMOs and the three lowest LUMOs for the ground states of complexes **1**–**4**.

[Re(Mebpy-CN)(CO)$_3$Cl] (**1**)					
MO	*E* [eV]	Re [%]	Me-bpyCN [%]	CO [%]	Cl [%]
LUMO+2	–1.54	2	92	6	1
LUMO+1	–2.23	0	99	1	0
LUMO	–3.10	2	92	4	1
HOMO	–6.72	49	4	21	25
HOMO–1	–6.82	47	6	20	27
HOMO–2	–7.30	68	1	31	0
$[Re(Mebpy\text{-}CN)(CO)_3(CH_3CN)]^+$, cation of **2**					
MO	*E* [eV]	Re [%]	Me-bpyCN [%]	CO [%]	AN [%]
LUMO+2	–1.73	2	91	6	0
LUMO+1	–2.40	0	99	1	0
LUMO	–3.29	2	93	4	0
HOMO	–7.29	60	10	25	5
HOMO–1	–7.40	61	10	23	5
HOMO–2	–7.62	69	2	29	0
$[(CH_3CN)(CO)_3Re(Mebpy\text{-}CN)Ru(NH_3)_5]^{3+}$, cation of **3**					
MO	*E* [eV]	Re [%]	Ru [%]	Me-bpyCN [%]	CO [%]
LUMO+2	–1.78	1	0	92	6
LUMO+1	–2.48	0	2	97	1
LUMO	–3.37	3	4	88	4
HOMO	–6.29	0	92	4	0
HOMO–1	–6.30	1	86	10	0
HOMO–2	–6.36	0	88	9	0
$[(CH_3CN)(CO)_3Re(Mebpy\text{-}CN)Ru(NH_3)_5]^{4+}$, cation of **4**					
α-MO	*E* [eV]	Re [%]	Ru [%]	Me-bpyCN [%]	CO [%]
LUMO+2	–2.79	0	1	97	1
LUMO+1	–3.16	0	59	0	0
LUMO	–3.78	3	2	92	3
HOMO	–7.03	62	0	11	21
HOMO–1	–7.33	62	0	10	21
HOMO–2	–7.48	71	0	2	26
$[(CH_3CN)(CO)_3Re(Mebpy\text{-}CN)Ru(NH_3)_5]^{4+}$, cation of **4**					
β-MO	*E* [eV]	Re [%]	Ru [%]	Me-bpyCN [%]	CO [%]
LUMO+2	–2.87	0	62	0	0
LUMO+1	–3.77	3	2	91	3
LUMO	–5.53	0	96	1	0
HOMO	–7.03	62	0	11	16
HOMO–1	–7.32	62	1	10	18
HOMO–2	–7.48	71	0	2	26

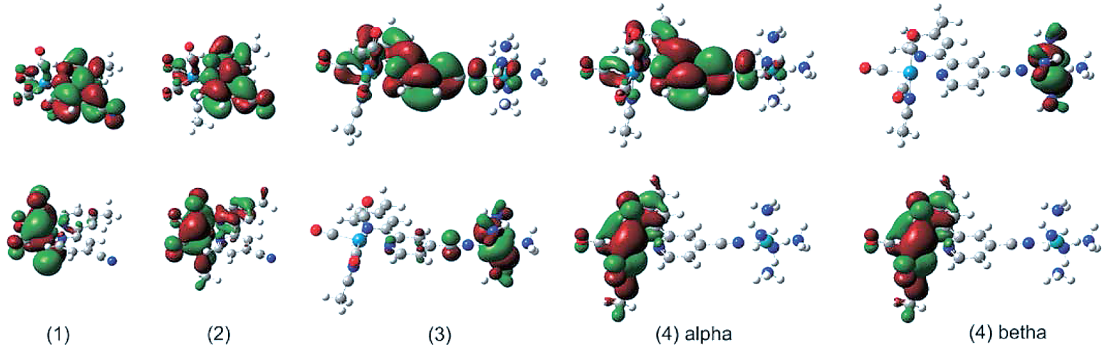

Figure 8. Electronic-density diagrams of some LUMOs (upper graphs) and HOMOs (lower graphs) for complexes **1**–**4**.

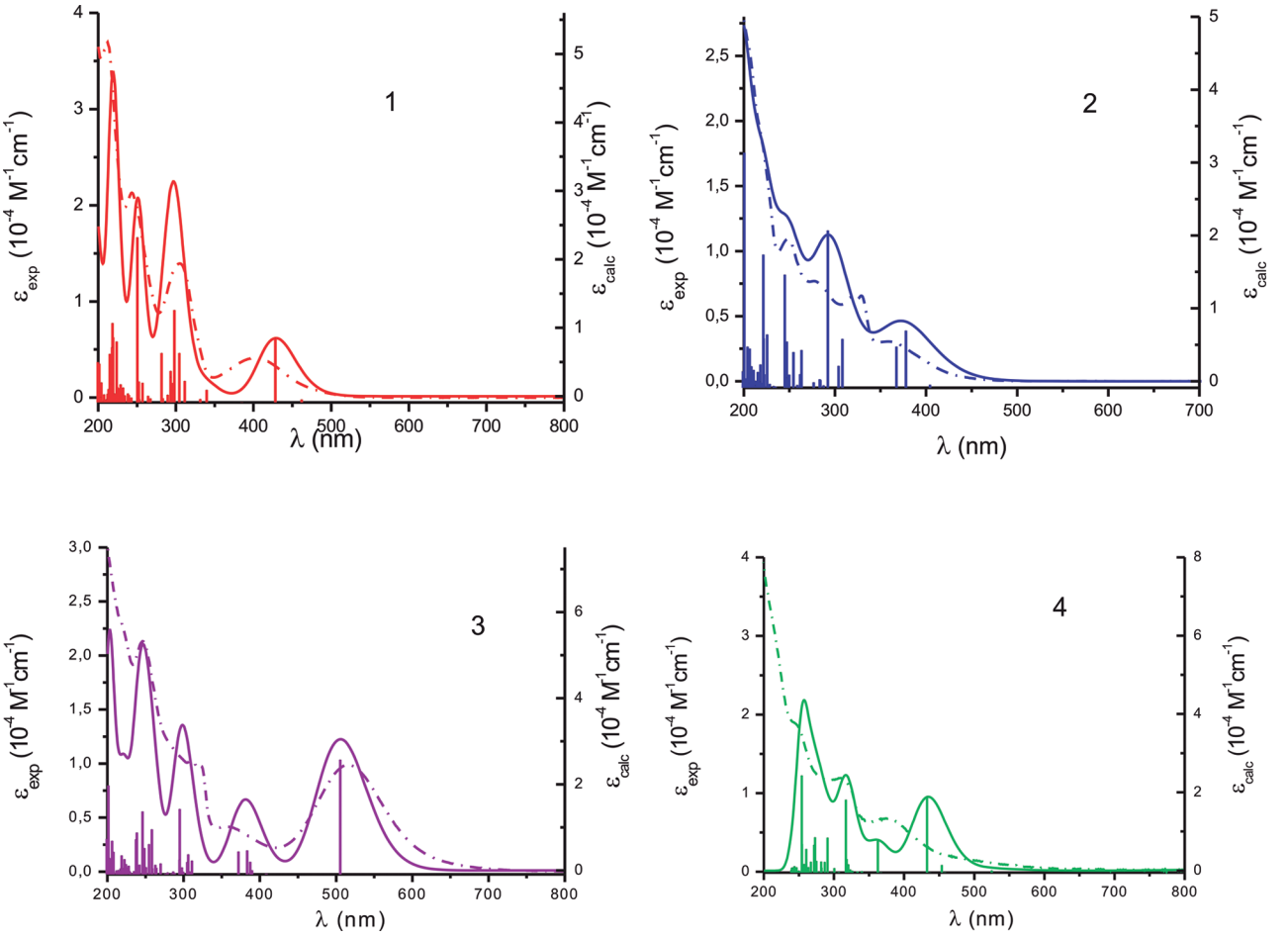

Figure 9. Calculated UV/Vis spectra of **1**–**4** in solid lines; experimental spectra in dashed lines.

As shown in Figure 9, calculated UV/Vis spectra for complexes **1**–**4** present reasonable agreement with the experimental spectra.

Conclusion

Novel mono- and dinuclear tricarbonylrhenium(I) complexes with Mebpy-CN were prepared and characterized by diffraction, spectroscopic, photophysical, and computational techniques. The increased conjugation in the bipyridyl ring due to the nitrile substituent increases the emission quantum yields of the ^{3}MLCT lowest-lying excited states with respect to the corresponding bpy complexes. In the mixed-valent species of formula $[(CH_3CN)(CO)_3Re(Mebpy\text{-}CN)Ru(NH_3)_5]^{4+}$, charge recombination from its MMCT excited state is predicted to lie in the Marcus inverted region. The electronic structures and optical properties of all the reported complexes calculated by DFT and TD-DFT methods agree reasonably well with experimental results.

Experimental Section

Materials and Instrumentation: All chemicals used in this work were analytical reagent grade. CH_3CN was freshly distilled from P_4O_{10} for electrochemical measurements. TBAH was recrystallized four times from EtOH and dried at 150 °C for 72 h. NMR spectra were obtained from samples in CD_3CN with a Bruker 500 MHz instrument operating at a frequency of 500.13 MHz for ^{1}H NMR spectroscopy and 125.75 MHz for ^{13}C NMR spectroscopy. ESI mass spectra were recorded with a Bruker Esquire 6000 mass spectrometer. Absorption spectra were determined with a Varian Cary 50 spectrophotometer using 1 cm quartz cells. Emission measurements for Ar-degassed solutions were carried out in 1 cm fluorescence cells with a Shimadzu RF-5301 PC spectrofluorometer at room temperature, and the spectra were corrected by a previously described procedure.[26] A cold finger Dewar accessory was used for emission measurements at 77 K. Ground-state infrared spectra (4000–400 cm^{-1}) were measured as KBr pellets with a Perkin–Elmer FTIR RX-I spectrophotometer. Raman spectra were recorded in the range 3500–60 cm^{-1} with a Raman DXR spectrometer from Thermo Scientific equipped with a trinocular Olympus Microscope. Electrochemical measurements were carried out with a BAS Epsilon EC instrument. A standard three-electrode arrangement was used, with vitreous carbon as working electrode, Pt wire as auxiliary electrode, and Ag/AgCl (3 M KCl) as reference electrode. All solutions were prepared in freshly distilled CH_3CN (with 0.1 M TBAH as the supporting electrolyte) and thoroughly degassed with Ar prior to each measurement. Reported $E_{1/2}$ values for reversible waves were calculated as the averages between the peak values that corresponded to the cathodic (E_c) and anodic (E_a) waves: $E_{1/2} = (E_c + E_a)/2$. Data obtained by CV were almost equal to those ob-

tained by differential pulse voltammetry (DPV). For irreversible waves, the reported values are those determined by DPV. UV/Vis spectroelectrochemical experiments were performed in CH_3CN (0.1 M TBAH) using a 1 mm path-length spectroelectrochemical cell from CH Instruments, with Pt grid as working electrode, Pt wire as counter electrode, and Ag/AgCl (3 M KCl) as reference electrode. Lifetimes and transient spectra of the lowest-lying ^{3}MLCT excited states were obtained with a laser flash photolysis setup as described previously.[1b] Lifetimes were also determined by a time-correlated single-photon counting (TCSPC) technique, with a Tempro-01 apparatus from Horiba Jobin Yvon (Glasgow, U.K.), using as the excitation pulse source an ultrafast (460±27) and (340±15) nm Nanoled from Horiba operating at 250 kHz. Emission was collected at the emission maxima of complexes **1**–**4** with a monochromator with emission bandwidth selected at 12 nm. Fluorescence intensity decay was fitted with the Fluorescence Decay Analysis Software DAS6 of Horiba Jobin Yvon by deconvolution of the pulse function using a single-exponential model function. All measurements were performed at room temperature in CH_3CN solutions saturated by bubbling for 20 min with high-purity argon, air, and oxygen gases (>99.98, Indura SRL, Argentina). Calculations were performed using Gaussian '98.[27] Molecules were optimized using the PBE1PBE hybrid functional, which is composed of the Perdew, Burke, Ernzerhof exchange,[28] and a correlation functional with 25% HF exchange. Basis set LanL2DZ was chosen for all atoms, and geometry optimizations were performed under vacuum. No symmetry restrictions were placed on the geometry optimizations. Frequency calculations were performed to ensure that these geometries corresponded to global minima: no imaginary frequencies were obtained for the optimized geometries. The effect of the solvent was included using the conductor-like polarizable continuum model (CPCM) for calculating orbital energy levels and UV/Vis spectra in acetonitrile. The contribution of the different groups on the orbitals, calculated UV/Vis spectra, and transitions related to them were obtained using the GaussSum Program (version 2.2).[29] UV/Vis profiles were obtained by considering a typical half-bandwidth of $\Delta\nu_{1/2}$ = 3000 cm^{-1} for all electronic transitions. Chemical analyses were carried out at INQUIMAE, University of Buenos Aires, Buenos Aires, Argentina, with an estimated error of ±0.5%.

Crystal Structure Determination: Crystals of **2** were obtained by slow evaporation of a concentrated solution of the complex in a acetonitrile/acetone/toluene/hexane (1:1:1:2) mixture. Measurements were carried out with a Bruker Smart Apex CCD diffractometer using graphite-monochromated Mo-K_a radiation (λ = 0.71073 Å) from an X-ray tube. The measurements were made in the range 2.086 to 28.350° for θ. Full-sphere data collection was carried out with ω and ϕ scans. A total of 21280 reflections were collected, of which 6525 [R(int) = 0.0301] were unique. The used programs were: SMART for data collection,[30] SAINT+ for data reduction,[31] SADABS for absorption correction.[32] Structure solution and refinement were carried out using SHELXTL.[33] The structure was solved by direct methods and refined by full-matrix least-squares methods on F^2. The non-hydrogen atoms were refined anisotropically. The hydrogen atoms were placed in geometrically optimized positions and forced to ride on the atom to which they are attached. Final R indices [$I > 2\sigma(I)$]: $R1$ = 0.269, $wR2$ = 0.0623. R indices (all data): $R1$ = 0.0304, $wR2$ = 0.0644.

Mebpy-CN: The ligand 4-methyl-2,2′-bipyridine-4′-carbonitrile (Mebpy-CN) was prepared following procedures reported in the literature.[34]

[Re(Mebpy-CN)(CO)$_3$Cl] (1): A mixture of [Re(CO)$_5$Cl] (200 mg, 0.553 mmol) and Mebpy-CN (112 mg, 0.574 mmol) was added to toluene (15 mL) and heated under reflux conditions for 2 h under subdued light. The mixture was cooled to room temperature and stored in the refrigerator at 5 °C for 1 h. The solid was then filtered, washed with toluene and diethyl ether, and dried under vacuum over P_4O_{10} overnight, yield 230 mg (83%). $C_{15}H_9ClN_3O_3Re$ (500.91): calcd. C 36.0, H 1.8, N 8.4; found C 36.1, H 1.8, N 8.3. ^{1}H NMR (500.13 MHz, CD_2Cl_2): δ = 2.61 (s, 3 H), 7.47 (1 H), 7.75 (1 H), 8.07 (1 H), 8.42 (1 H), 8.88 (1 H), 9.20 (1 H) ppm. ESI MS ion clusters at m/z = 523.77 [M – Cl – CO + CD_2Cl_2]$^+$. ESI MS negative ion clusters at m/z 553.75 {[Re(Mebpy-CN)(CO)$_3$Cl$_2$(H$_2$O)]}$^-$. IR (KBr): $\tilde{\nu}$ = 3050 (vw), 2935 (vw), 2226 (w), 2244 (vw), 2025 (vs), 1938 (vs) 1880(vs) 1618(w), 1410 (w) cm^{-1}. UV/Vis (CH_3CN): λ ($\varepsilon \times 10^{-4}$, M^{-1} cm^{-1}) = 212 (3.70), 243 (2.13), 305 (1.40), 402 (0.41) nm.

[Re(Mebpy-CN)(CO)$_3$(CH$_3$CN)][(PF$_6$)·3.5H$_2$O (2): $AgCF_3SO_3$ (77 mg, 0.300 mmol) was added to a solution of **1** (145 mg, 0.289 mmol) in CH_3CN (80 mL) and heated under reflux conditions for 4.5 h under subdued light. The mixture was then cooled to room temperature, and a stoichiometric quantity of AgCl was removed by filtration. The filtrate was rotary evaporated to approximately 5 mL and added to a solution of NH_4PF_6 (370 mg) in water (4 mL). After cooling in the refrigerator overnight, the yellow solid was filtered, washed with water and diethyl ether, and dried under vacuum. The solid was subjected to flash chromatography on silica gel (with toluene/acetone/methanol: 6:3:1) and the first eluent was collected. The solution was rotary evaporated to dryness and the obtained solid was collected with acetone (5 mL), added to *n*-hexane (50 mL), and stored in the freezer overnight. The obtained light yellow solid was filtered and dried under vacuum over P_4O_{10} overnight, yield 150 mg (76%). $C_{17}H_{15}F_6N_4O_{4.5}P_1Re$ (678.5): calcd. C 30.1, H 2.2, N 8.3; found C 30.4, H 1.8, N 7.7. ^{1}H NMR (500.13 MHz, CD_3CN): δ = 2.04 (br. s, 3 H), 2.61 (s, 3 H), 7.62 (1 H), 7.97 (1 H), 8.38 (1 H), 8.78 (1 H), 8.87 (1 H), 9.18 (1 H) ppm. ^{13}C NMR (125.75 MHz, CD_3CN): δ = 3.92, 21.7, 116.2, 123.8, 125.0, 127.0, 127.5, 130.4, 130.7, 154.6, 2×155.2, 156.1, 158.7, 3×194.5 ppm. ESI MS ion clusters at m/z = 506.80 [Re(Mebpy-CN)(CO)$_3$(CH$_3$CN)]$^+$, 509.82 [Re(Mebpy-CN)(CO)$_3$(CD$_3$CN)]$^+$. IR (KBr pellet): $\tilde{\nu}$ = 3096 (vw), 2958 (vw), 2298 (vw), 2240 (vw), 2041 (vs), 1941 (vs) 1930(vs), 1618 (w), 1411 (w), 845 (vs), 557 (m) cm^{-1}. UV/Vis (CH_3CN): λ ($\varepsilon \times 10^{-4}$, M^{-1} cm^{-1}) = 248 (1.09), 318 (0.65), 329 (0.66), 360 (0.31) nm.

[(CH$_3$CN)(CO)$_3$Re^{I}(Mebpy-CN)Ru^{II}(NH$_3$)$_5$][(PF$_6$)$_3$ (3): A solution of **2** (50 mg, 0.070 mmol) in acetone (20 mL) was purged with Ar for 30 min. Then [Ru(NH$_3$)$_5$(H$_2$O)][(PF$_6$)$_2$ (35 mg, 0.070 mmol), which was prepared according to a reported method,[35] was added, and the resulting mixture was stirred under Ar for 4 h. The final purple solution was concentrated to approximately 5 mL, and diethyl ether (50 mL) was added to precipitate a purple solid that was stored overnight. The solid was filtered, rinsed with diethyl ether, and purified by chromatography in alumina (acetone/methanol, 1:1). Unreacted mononuclear precursor eluted first, and the new dinuclear complex was collected afterward, rotary evaporated to approximately 5 mL, precipitated by diethyl ether, and stored in the refrigerator overnight. Finally, a purple solid was filtered and dried under vacuum over P_4O_{10}, yield 34 mg (43%). $C_{17}H_{27}F_{18}N_9O_3P_3ReRu$ (1127.6): calcd. C 18.1, H 2.4, N 11.2; found C 17.9, H 2.5, N 11.3. ^{1}H NMR (500.13 MHz, CD_3CN): δ = 2.07 (3 H,), 2.60 (s, 3 H), 7.56 (1 H), 7.77 (1 H), 8.30 (1 H), 8.61 (1 H), 8.89 (1 H), 9.11 (1 H) ppm. ^{13}C NMR (125.75 MHz, CD_3CN): δ = 21.7, 116.5, 123.8, 125.6, 126.1, 127.6, 129.8, 130.0, 2×154.6, 155.9, 158.3, 194.5 ppm. ESI MS ion clusters at m/z = 506.80 [M – Ru(NH$_3$)$_5$(PF$_6$)$_3$]$^+$, 538.89 [M – Re(CO)$_3$(CH$_3$CN)(PF$_6$)$_2$]$^+$. IR (KBr pellet): $\tilde{\nu}$ = 3371 (m), 3300 (m), 3186

(vw), 2958 (vw), 2933 (vw), 2269 (vw), 2179 (s), 2026 (vs), 1935 (vs), 1898 (vs), 1608 (s), 1413 (w), 1278 (s), 839 (vs), 559 (s) cm^{-1}. UV/Vis (CH_3CN): λ ($\varepsilon \times 10^{-4}$, $M^{-1}cm^{-1}$) = 247 (2.13), 310 (1.03), 323 (0.98), 358 (0.41), 516 (0.99) nm.

$[(CH_3CN)(CO)_3Re^{I}(Mebpy\text{-}CN)Ru^{III}(NH_3)_5](PF_6)_3Br\cdot 12H_2O$ (4): A solution of **3** (20 mg) in freshly distilled acetonitrile (10 mL) was oxidized by the addition of a stoichiometric amount of a standardized solution of Br_2 in acetonitrile.[36] The complex was precipitated by the addition of diethyl ether (100 mL) and stored in the refrigerator overnight. An orange solid was filtered, washed three times with diethyl ether, and dried under vacuum. It was recrystallized from acetone/diethyl ether, filtered, and dried under vacuum over P_2O_4, yield 34 mg (43%). $C_{17}H_{51}BrF_{18}N_9O_{15}P_3ReRu$ (1423.7): calcd. C 14.3, H 3.6, N 8.9; found C 14.0, H 3.3, N 9.0. IR (KBr pellet): $\tilde{\nu}$ = 3348 (m), 3244 (m), 3186 (vw), 2936 (vw), 2293 (vw), 2241 (vw), 2038 (vs), 1943 (vs) 1904(vs) 1623(m), 1419 (m), 1312 (m), 839 (vs), 559 (s) cm^{-1}.

CCDC-977825 contains the supplementary crystallographic data for this paper. These data can be obtained free of charge from The Cambridge Crystallographic Data Centre via www.ccdc.cam.ac.uk/data_request/cif.

Supporting Information (see footnote on the first page of this article): Crystal data in Table S1, selected bond lengths and angles in Table S2, emission spectral fittings in Table S3, spectroelectrochemistry of complex **1** in Figure S1, comparisons of IR spectra of **1** and its hydrolyzed derivative in Figure S2, hydrolysis consecutive spectra in Figure S3, and crystallographic data in cif format.

Acknowledgments

Dr. Miriam Pérez-Trujillo (UAB) is thanked for MS measurements. The authors also thank the Universidad Nacional de Tucumán (UNT), Universidad Nacional de Santiago del Estero (UNSE), Consejo Nacional de Investigaciones Científicas y Técnicas (CONICET), Agencia Nacional de Promoción Científica y Tecnológica (ANPCyT), all from Argentina, and the Spanish Ministerio de Economía y Competitividad (MINECO) (project number CTQ2012-32436) for financial support. J. H. M. O. thanks CONICET for a graduate fellowship. F. E. M. V., C. D. B., F. F., and N. E. K. thank CONICET, Argentina, as Members of the Research Career.

[1] a) M. Cattaneo, F. Fagalde, N. E. Katz, *Inorg. Chem.* **2006**, *45*, 6884–6891; b) M. Cattaneo, F. Fagalde, N. E. Katz, C. D. Borsarelli, T. Parella, *Eur. J. Inorg. Chem.* **2007**, 5323–5332.
[2] G. Pourrieux, F. Fagalde, I. Romero, X. Fontrodona, T. Parella, N. E. Katz, *Inorg. Chem.* **2010**, *49*, 4084–4091.
[3] A. J. Amoroso, M. P. Coogan, J. E. Dunne, V. Fernández-Moreira, J. B. Hess, A. J. Hayes, D. Lloyd, C. Millet, S. J. A. Pope, C. Williams, *Chem. Commun.* **2007**, 3066–3068.
[4] V. W.-W. Yam, C.-C. Ko, N. Zhu, *J. Am. Chem. Soc.* **2004**, *126*, 12734–12735.
[5] H. Takeda, O. Ishitani, *Coord. Chem. Rev.* **2010**, *254*, 346–354.
[6] F. Fagalde, M. E. García Posse, M. M. Vergara, M. Cattaneo, N. E. Katz, I. Romero, T. Parella, A. Llobet, *Polyhedron* **2007**, *26*, 17–23.
[7] J. H. Mecchia Ortiz, N. Vega, D. Comedi, M. Tirado, I. Romero, X. Fontrodona, T. Parella, F. E. Morán Vieyra, C. D. Borsarelli, N. E. Katz, *Inorg. Chem.* **2013**, *52*, 4950–4962.
[8] R. Lin, Y. Fu, C. Brock, T. F. Guarr, *Inorg. Chem.* **1992**, *31*, 4346–4353.
[9] C. A. Hunter, J. K. M. Sanders, *J. Am. Chem. Soc.* **1990**, *112*, 5525–5534.
[10] F. H. Allen, O. Kennard, D. G. Watson, L. Brammer, A. G. Orpen, R. Taylor, *J. Chem. Soc. Perkin Trans. 2* **1987**, S1–S19.
[11] K. Nakamoto, *Infrared and Raman Spectra of Inorganic and Coordination Compounds*, 4th ed., Wiley, New York, **1986**.
[12] L. A. Worl, R. Duesing, P. Chen, L. Della Ciana, T. J. Meyer, *J. Chem. Soc., Dalton Trans.* **1991**, 849–858.
[13] M. G. Mellace, F. Fagalde, N. E. Katz, I. G. Crivelli, A. Delgadillo, A. M. Leiva, B. Loeb, M. T. Garland, R. Baggio, *Inorg. Chem.* **2004**, *43*, 1100–1107.
[14] a) J. P. Bullock, E. Carter, R. Johnson, A. T. Kennedy, S. E. Key, B. J. Kraft, D. Saxon, P. Underwood, *Inorg. Chem.* **2008**, *47*, 7880–7887; b) A. Klein, C. Vogler, W. Kaim, *Organometallics* **1996**, *15*, 236–244.
[15] E. S. Dodsworth, A. B. P. Lever, *Chem. Phys. Lett.* **1984**, *112*, 567–570.
[16] F. Fagalde, M. G. Mellace, N. D. Lis de Katz, N. E. Katz, *J. Coord. Chem.* **2004**, *57*, 635–639.
[17] C. Creutz, *Prog. Inorg. Chem.* **1983**, *30*, 1–73.
[18] N. E. Katz, C. Creutz, N. Sutin, *Inorg. Chem.* **1988**, *27*, 1687–1694.
[19] R. A. Marcus, N. Sutin, *Biochem. Biophys. Acta* **1985**, *811*, 265–322.
[20] K. Suzuki, A. Kobayashi, S. Kaneko, K. Takehira, T. Yoshihara, H. Ishida, Y. Shiina, S. Oishi, S. Tobita, *Phys. Chem. Chem. Phys.* **2009**, *11*, 9850–9860.
[21] J. V. Caspar, T. D. Westmoreland, G. H. Allen, P. G. Bradley, T. J. Meyer, W. H. Woodruff, *J. Am. Chem. Soc.* **1984**, *106*, 3492–3500.
[22] C. E. McCusker, J. K. McCusker, *Inorg. Chem.* **2011**, *50*, 1656–1669.
[23] S. Sato, Y. Matubara, K. Koike, M. Falkenström, T. Katayama, Y. Ishibashi, H. Miyasaka, S. Taniguchi, H. Chosrowjan, N. Mataga, N. Fukazawa, S. Koshihara, K. Onda, O. Ishitani, *Chem. Eur. J.* **2012**, *18*, 15722–15734.
[24] a) N. E. Katz, S. L. Mecklenburg, D. K. Graff, P. Chen, T. J. Meyer, *J. Phys. Chem.* **1994**, *98*, 8959–8961; b) N. E. Katz, S. L. Mecklenburg, T. J. Meyer, *Inorg. Chem.* **1995**, *34*, 1282–1284.
[25] a) A. Vlček Jr, S. Záliš, *J. Phys. Chem. A* **2005**, *109*, 2991–2992; b) J. A. Pople, P. M. W. Gill, N. C. Handy, *Int. J. Quantum Chem.* **1995**, *56*, 303–305.
[26] J. R. Lakowicz, *Principles of Flourescence Sectroscopy*, 3rd ed., Springer, New York, **2006**.
[27] M. J. Frisch, G. W. Trucks, H. B. Schlegel, G. E. Scuseria, M. A. Robb, J. R. Cheeseman, V. G. Zakrzewski, J. A. Montgomery, R. E. Stratman, J. C. Burant, S. Dapprich, J. M. Millam, A. D. Daniels, K. N. Kudin, M. C. Strain, O. Farkas, J. Tomasi, V. Barone, M. Cossi, R. Cammi, B. Menucci, C. Pomelli, C. Adamo, S. Clifford, J. Ochterski, G. A. Petersson, P. Y. Ayala, Q. Cui, K. Morokuma, D. K. Malick, A. D. Rabuck, K. Raghavachari, J. B. Foresman, J. Cioslovski, J. V. Ortiz, B. B. Stefanov, G. Liu, A. Liashenko, P. Piskorz, I. Komaromi, R. Gomperts, R. L. Martin, D. J. Fox, T. Keith, M. A. Al-Laham, C. Y. Peng, A. Nanayakkara, C. Gonzales, M. Challacombe, P. M. W. Gill, B. Johnson, W. Chen, M. W. Wong, J. L. Andres, C. Gonzales, M. Head-Gordon, E. S. Replogle, J. A. Pople, *Gaussian 98*, Revision A.6, Gaussian, Inc., Pittsburgh, PA, **1998**.
[28] J. P. Perdew, K. Burke, M. Ernzerhof, *Phys. Rev. Lett.* **1996**, *77*, 3865–3868.
[29] N. M. O'Boyle, A. L. Tenderholt, K. M. Langner, J. Comp. Chem. **2008**, 29, 839–845. Available from: http://gausssum.sf.net.
[30] *SMART*, version 5.631, Bruker AXS Inc., Madison, WI, **1997–2002**.
[31] *SAINT+*, version 6.36A, Bruker AXS Inc., Madison, WI, **2001**.
[32] G. M. Sheldrick, *Empirical Absorption Correction Program*, Universität Göttingen, Germany, **1996**; Bruker Advanced X-ray Solutions, *SADABS*, version 2.10, **2001**.

[33] G. M. Sheldrick, Program for Crystal Structure Refinement, Universität Göttingen, Germany, **1997**; Bruker Advanced X-ray Solutions, *SHELXTL*, version 6.14, **2000**–**2003**.
[34] a) G. Vériot, J.-P. Dutasta, G. Matouzenko, A. Collet, *Tetrahedron* **1995**, *51*, 389–400; b) J. P. Kirby, J. A. Roberts, D. G. Nocera, *J. Am. Chem. Soc.* **1997**, *119*, 9230–9236.
[35] J. E. Sutton, H. Taube, *Inorg. Chem.* **1981**, *20*, 3125–3134.
[36] M. J. Powers, R. W. Callahan, D. J. Salmon, T. J. Meyer, *Inorg. Chem.* **1976**, *15*, 894–900.

Received: March 10, 2014
Published Online: June 13, 2014

